MESH-INDEPENDENT LARGE-EDDY SIMULATION WITH ANISOTROPIC ADAPTIVE MESH REFINEMENT FOR HYDROGEN DEFLAGRATION PREDICTION IN CLOSED VESSELS

Taylor, R.[1], Groth, C. P. T. [1], Liang Z.[2] and Ivan L.[2]
[1] University of Toronto Institute for Aerospace Studies, Canada
[2] Canadian Nuclear Laboratories, Chalk River, Ontario, K0J 1J0, Canada
***Corresponding author*: ryanc.taylor@mail.utoronto.ca**

ABSTRACT

The use of high-fidelity simulation methods based on large-eddy simulation (LES) are proving useful for understanding and mitigating the safety hazards associated with hydrogen releases from nuclear power plants. However, accurate modeling of turbulent premixed hydrogen flames via LES can require very high resolution to capture both the large-scale turbulence and its interaction with the flame fronts. Standard meshing strategies can result in impractically high computational costs, especially for the thin fronts of hydrogen flames. For these reasons, the use of a recently formulated integral length scale approximation (ILSA) subfilter-scale model, in combination with an efficient anisotropic block-based adaptive mesh refinement (AMR) technique is proposed and examined herein for performing LES of turbulent premixed hydrogen flames. The anisotropic AMR method allows dynamic and solution-dependent resolution of flame fronts and the grid-independent properties of the ILSA model ensure that numerical errors associated with implicitly-filtered LES techniques in regions with varying resolution are avoided. The combined approach has the potential to allow formally converged LES solutions (direct numerical simulation results are typically reached in the limit of very fine meshes with standard subgrid models). The proposed LES methodology is applied to combustion simulations of lean premixed hydrogen-air mixtures within closed vessels: a problem relevant to hydrogen safety applications in nuclear facilities. A progress variable-based method with a multi-phenomena burning velocity model is used as the combustion model. The present simulation results are compared to the available experiment data for several previously studied THAI vessel cases and the capabilities of the proposed LES approach are assessed.

1.0 INTRODUCTION AND MOTIVATION

The accurate prediction of turbulent premixed hydrogen flames in closed vessels is beneficial in a number of safety related fields, including the assessment of the hazards of hydrogen combustion within the containment building of a nuclear power plant. The use of three-dimensional (3D) computational fluid dynamics (CFD) methods has proven useful in this regard, with many organizations and studies adopting such methods to perform high-fidelity detailed simulations of hydrogen release and combustion under postulated accident conditions [1].

The widespread application of large-eddy simulation (LES) to hydrogen combustion in nuclear containments has been limited by the high-resolution requirements for capturing the flame front and flame brush to accurately predict large-scale flame wrinkling and propagation. Unfortunately, computationally tractable, static, numerical meshes are usually not fine enough to sufficiently resolve the critical length scales associated with practical configurations. For instance, the computational cost incurred by static meshes to resolve the width of the flame brush that is on the order of milli- or micro-meters in a vessel on the order of meters is generally prohibitive. Therefore, the use of adaptive mesh refinement (AMR) [2, 3], wherein the mesh is dynamically refined and coarsened depending on the local solution content to accurately treat the required regions of the flow while reducing the overall computational cost, is an attractive alternative for LES of reactive flows. However, the use of mesh-dependent LES subfilter-scale (SFS) turbulence models, such as the popular Smagorinsky model, can cause problems when used in conjunction with AMR or even with static meshes featuring varying cell sizes [4]. Specifically, mesh-dependent LES SFS models tie the SFS viscosity directly to the cell volume, which can lead to sharp changes in the unresolved fluctuating quantities with cells of largely different sizes. These undesirable sudden changes can introduce significant numerical error and even instabilities into the simulation [4], thereby negatively impacting the quality of the LES results.

In this study, a novel block-based anisotropic AMR scheme [3, 5, 6, 7, 2] is applied in conjunction with a recently proposed mesh-independent integral length scale approximation (ILSA) SFS model [8] to the LES of turbulent premixed hydrogen flames in closed vessels. In particular, the simulation of a number of the well-studied THAI experiments [1] is considered to evaluate the computational benefits of the new approach. The LES results of the premixed hydrogen flames obtained using the combined AMR/ILSA approach are compared to results from the original experiments, as well as to other LES results obtained using the mesh-dependent Smagorinsky SFS model [9].

In what follows, details of the proposed anisotropic AMR and finite-volume schemes for solution of the Favre-filtered Navier-Stokes equations governing turbulent flows of a fully-compressible reactive mixture on 3D, multi-block, body-fitted, computational mesh consisting of hexahedral volume elements are described along with additional details of the ILSA SFS and multi-phenomena burning velocity combustion model. The latter is adopted here to model the interaction between turbulence and chemistry and thermal-diffusive instabilities of the hydrogen flames. The LES results are then compared to available measured data for several THAI experiments. The performance of the combined anisotropic AMR and ILSA approach is assessed.

2.0 LES COMBUSTION MODELLING AND GOVERNING EQUATIONS

The LES modelling approach adopted herein follows closely the framework developed and applied successfully in previous LES studies of premixed flames by Hernandez-Perez *et al.* [10, 11] and Shahbazian *et al*. [12].

2.1 Favre-Filtered Governing Equations

The Favre-filtered form of the Navier-Stokes equations governing compressible flows of a thermally perfect reactive gaseous mixture is used herein to describe the turbulent premixed combustion processes. Dufour, Soret and radiation effects are neglected. The transport equations for the mixture mass, momentum, energy, and species concentrations can be written as

$$\frac{\partial \bar{\rho}}{\partial t} + \frac{\partial (\bar{\rho}\tilde{u}_i)}{\partial x_i} = 0, \tag{1}$$

$$\frac{\partial (\bar{\rho}\tilde{u}_i)}{\partial t} + \frac{\partial \left(\bar{\rho}\tilde{u}_i\tilde{u}_j + \delta_{ij}\bar{p}\right)}{\partial x_j} - \frac{\partial \check{\tau}_{ij}}{\partial x_j} = \bar{\rho} g_i - \frac{\partial \sigma_{ij}}{\partial x_j}, \tag{2}$$

$$\frac{\partial (\bar{\rho}\tilde{E})}{\partial t} + \frac{\partial [(\bar{\rho}\tilde{E}+\bar{p})\tilde{u}_i]}{\partial x_i} - \frac{\partial (\check{\tau}_{ij}\tilde{u}_j)}{\partial x_i} + \frac{\partial \check{q}_i}{\partial x_i} = \bar{\rho}\tilde{u}_i g_i - \frac{\partial [\bar{\rho}(\widetilde{h_s u_\iota} - \tilde{h}_s\tilde{u}_i)]}{\partial x_i} - \frac{\partial [\bar{\rho}(u_i\widetilde{u_j}u_J - \tilde{u}_i\tilde{u}_j\tilde{u}_j)]}{\partial x_i} - \frac{1}{2}\frac{\partial \left[\sum_{n=1}^{N_{species}} \Delta h_{f,n}^0 \bar{\rho}(\widetilde{Y_n u_\iota} - \widetilde{Y_n}\tilde{u}_i)\right]}{\partial x_i}, \tag{3}$$

$$\frac{\partial (\bar{\rho}\tilde{Y}_n)}{\partial t} + \frac{\partial \left(\bar{\rho}\tilde{Y}_n\tilde{u}_j\right)}{\partial x_i} - \frac{\partial J_{n,i}}{\partial x_i} = \frac{\partial [\bar{\rho}(\widetilde{Y_n u_\iota} - \tilde{Y}_n\tilde{u}_i)]}{\partial x_i} + \bar{\dot{\omega}}_n, \tag{4}$$

where ρ is the mixture density, u_i is the mixture velocity vector, p is the pressure, τ_{ij} is the fluid stress tensor, g_i is the acceleration vector due to gravity, E is the total energy of the mixture, q_i is the heat flux vector, and Y_n, $J_{n,i}$ and $\dot{\omega}_n$ are the mass fraction, the mass flux relative to the mixture, and the reaction rate for species n, respectively. An overbar "-" represents a filtered quantity, a tilde "~" represents a Favre-filtered quantity, and a chevron "ˇ" represents a quantity evaluated in terms of filtered quantities. Additionally, σ_{ij} is SFS stress tensor, h_s is the sensible enthalpy, $\Delta h_{f,n}^0$ is the heat of formation for species n, and $\delta_{ij}$is the Kronecker delta function. Modelling of the LES SFS stress tensor, σ_{ij}, and a number of the other high-order correlations appearing above is required for closure of this filtered equation set.

2.2 SFS Turbulence Stress Model

Both the ILSA and standard Smagorinsky models are used herein to evaluate the SFS stress tensor, σ_{ij}. These models make use of an eddy viscosity approach, wherein the unclosed SFS stress tensor takes the form [8, 9]

$$\sigma_{ij} - \frac{\delta_{ij}}{3}\sigma_{kk} = -2\bar{\rho}\,\nu_{SFS}\left(\check{S}_{ij} - \frac{\delta_{ij}}{3}\check{S}_{kk}\right), \tag{5}$$

where $\check{S}_{ij}$ is the resolved rate of strain tensor and ν_{SFS} is the SFS turbulent viscosity. In the Smagorinsky model [9], the SFS viscosity is approximated using

$$\nu_{SFS} = (C_s\Delta)^2\left|\check{S}_{ij}\right|, \tag{6}$$

where Δ is the filter width and C_s is the usual Smagorinsky constant. The filter width is generally defined to be proportional to the cubic root of the volume of the local cell; it is this link between the SFS viscosity and the mesh spacing that can cause issues when used on non-uniform meshes. The ILSA model was developed specifically as a mesh independent SFS LES model [8]. It makes use of the same eddy viscosity approach given in Eq. (5), but differs in the evaluation of SFS turbulent viscosity as

$$\nu_{SFS} = (C_k L_{est})^2\left|\check{S}_{ij}\right|, \tag{7}$$

where C_k is a model coefficient and L_{est} is an estimate of the integral length scale of the turbulence, which can be represented as

$$L_{est} = \frac{\langle K_{res}\rangle^{\frac{3}{2}}}{\langle \varepsilon_{tot}\rangle}, \tag{8}$$

where K_{res} is the resolved turbulent kinetic energy and ε_{tot} is the total (sum of resolved and SFS) dissipation. Angled brackets represent averaged quantities, either spatially over homogeneous planes or directions, or temporally where no spatial homogeneity exists. Since no homogeneous spatial directions are expected for the present closed vessel simulations, temporal averaging was used herein to find the averaged quantities by using the local large-eddy turnover time as the averaging period. The model coefficient, C_k, is found by solving locally a quartic equation and its value is dependent on a target level for the modelled turbulence relative to the total. Thus, the ILSA model remains active even as the mesh is refined.

2.3 Flamelet-Based Combustion Model

In order to model the interaction between the chemical kinetics and turbulence and to specify the filtered reaction rates for the premixed flame of interest here, a standard flamelet-based combustion model is applied. In this approach, rather than solving directly for the species mass fractions, a reaction progress variable, *c*, is introduced based on the mass fraction of the fuel in the burned and unburned states. Thus, *c*=0 corresponds to a mixture of fresh (pure) reactants and *c*=1 to a mixture of burnt products. The treatment of the chemical kinetics is then reduced to solving a single filtered transport equation for the reaction progress variable, which takes the form [12]

$$\frac{\partial(\bar{\rho}\tilde{c})}{\partial t} + \frac{\partial\left(\bar{\rho}\tilde{c}\tilde{u}_j\right)}{\partial x_i} + \frac{\partial[\bar{\rho}(\widetilde{cu}_i - \tilde{c}\tilde{u}_i)]}{\partial x_i} = \bar{\dot{\omega}}_c + \overline{\frac{\partial}{\partial x_i}\left(\rho D_c \frac{\partial c}{\partial x_i}\right)}, \tag{9}$$

where D_c is the molecular diffusion coefficient and $\bar{\dot{\omega}}_c$ is the filtered net rate of production of the progress variable. Following the empirical burning velocity model (BVM) [13], the combined filtered chemical reaction rate and molecular diffusion terms are modeled as

$$\bar{\dot{\omega}}_c + \overline{\frac{\partial}{\partial x_i}\left(\rho D_c \frac{\partial c}{\partial x_i}\right)} = \rho_u s_t |\nabla \tilde{c}|, \quad s_t = \Xi s_l, \tag{10}$$

where ρ_u is the reactant density and s_t is the modeled turbulent flame speed. The latter is evaluated by applying a multiplicative factor, Ξ, that accounts for flame wrinkling, thermodiffusive, and initial turbulence effects, to the laminar flame speed s_l. The laminar flame speed is determined herein *a priori* by using the Cantera software package [14] in conjunction with the chemical mechanism of Alekseev *et al.* [15] for hydrogen and air, which involves 9 chemical species and 20 reactions. To account for the changing conditions within the vessel during the combustion process, the laminar flame speed was computed at a range of pressures between 1.25 and 7 atmospheres, with the temperature and density of the gas varying according to isentropic compression. During the simulation, values for the laminar flame speed are interpolated directly from a tabulated set of these values while the density of the unburned mixture, ρ_u, is computed according to the assumption of isentropic compression.

3.0 BLOCK-BASED ANISOTROPIC AMR AND FINITE-VOLUME METHODS FOR LES

3.1 Finite-Volume Method

The governing LES equations outlined above are solved by applying a finite-volume spatial discretization procedure to each computational cell of a 3D multi-block body-fitted mesh composed of hexahedral volume elements. The finite-volume scheme [10, 11, 12] makes use of a piecewise limited linear solution reconstruction and Riemann solver-based flux functions in the evaluation of the inviscid solution fluxes and, for the viscous fluxes, a centrally-weighted scheme is adopted. For this study, the approximate Riemann solver of Roe [16] is used in the inviscid flux evaluation. A standard second-order Runge-Kutta explicit time marching scheme is used to integrate the non-linear system of first-order ordinary differential equations resulting from the finite-volume discretization procedure and evolve the solution within each computational cell forward in time.

3.2 Block-Based Anisotropic AMR

A flexible block-based hierarchical binary tree data structure is used in conjunction with the finite-volume spatial discretization procedure mentioned above to facilitate automatic solution-directed anisotropic mesh adaptation on body-fitted multi-block mesh. The general AMR framework of Freret and Groth [3, 5, 6, 7], based on extensions to the previous work by Williamschen and Groth [2], is adopted here. An example of a non-uniform block within a multi-block grid structure is given in Figure 1. Note that the neighboring cells are used directly as the ghost cells for each grid block, even those at different levels of refinement as found at grid resolution changes. With this structure, anisotropic mesh refinement and efficient and highly scalable parallel implementation are readily achieved via domain decomposition.

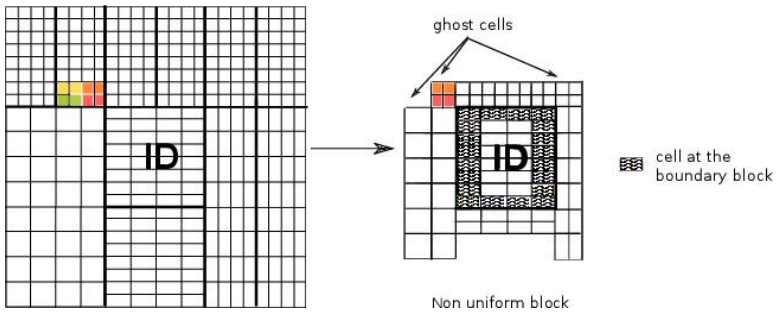

Figure 1. Example of a non-uniform structured mesh block (right) obtained from a block-based anisotropic AMR grid mesh (left).

In the anisotropic AMR scheme, mesh adaptation is accomplished by refining and coarsening of individual grid blocks. Figure 2 depicts a schematic of the resulting binary tree after several refinements of an initial mesh consisting of a single block. Each refinement produces new blocks called "children" from a "parent" block and the children can be refined further. This refinement process can be reversed in regions that are deemed over-resolved and two, four or eight children are coarsened or merged into a single parent block. The binary tree data structure is used for tracking block connectivity and mesh refinement history. Within this structure, each node of the binary tree stores references to two child nodes, corresponding to a grid block refinement in one of three coordinate directions. Local refinement and coarsening of the mesh is directed herein using physics-based refinement criteria based on the gradient of the progress variable. Directional dependent refinement criteria are based on the components of this gradient such that the mesh can be refined in an anisotropic way.

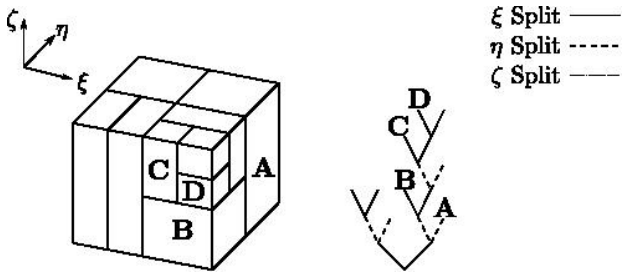

Figure 2. Schematic of 3D binary tree and the corresponding multi-block grid after several anisotropic refinements.

4.0 THAI EXPERIMENTS AND SETUP OF LES CASES

4.1 Experimental Cases of Interest

The THAI experiments [1] were performed using a vessel measuring 9.2 m tall by 3.2 m in diameter and filled with a hydrogen/air mixture. Ignition was trigged by a sparker located in either the bottom or top cylinder. A range of initial conditions (pressure, temperature, hydrogen & steam concentration, mixture uniformity) were considered in the THAI experiments and two of these cases were selected for the evaluation of the proposed approach; their experimental conditions, both specified and measured, are listed in Table 1.

The THAI vessel was equipped with four "fast" pressure transducers distributed along the vessel height, 43 "fast" thermocouples installed at 13 different elevations alongside a number of gas sampling lines [1]. The thermocouples were used to monitor the flame front propagation throughout the vessel. Experimental data pertaining to pressure and temperature were obtained from the original experiments. Comparisons between the experimental and predicted LES pressure rises, temperature histories, and flame propagation using this data are presented in Section 5.

Table 1. Summary of the initial conditions for the THAI experimental cases considered in this study [1]

Case	Pressure (bar)		Temperature (ºC)		Hydrogen Concentration (% by volume)		Steam Concentration (% by volume)	
	Spec.	Meas.	Spec.	Meas.	Spec.	Meas.	Spec.	Meas.
HD-15	1.5	1.505	90	92.5	10	9.93	0	0
HD-22	1.5	1.487	90	91.9	10	9.90	25	25.3

4.2 Summary of LES Simulations

Simulations were undertaken for each experiment on a static coarse mesh using the Smagorinsky and ILSA models. Two additional simulations, using both the ILSA and Smagorinsky models and a dynamic AMR mesh was undertaken for both cases as well. The details for each of these eight simulations, along with the selected nomenclature for distinguishing the cases, are summarized in Table 2.

Table 2. Summary of simulation cases

THAI Case	Simulation Name	Turbulence Model	Mesh Type	Maximum AMR Level	Maximum # of Cells
HD-15	HD15-IA2	ILSA	Dynamic AMR	2	800,000
	HD15-IC	ILSA	Static Coarse	-	77,760
	HD15-SA2	Smagorinsky	Dynamic AMR	2	900,000
	HD15-SC	Smagorinsky	Static Coarse	-	77,760
HD-22	HD22-IA2	ILSA	Dynamic AMR	2	800,000
	HD22-IC	ILSA	Static Coarse	-	77,760
	HD22-SA2	Smagorinsky	Dynamic AMR	2	900,000
	HD22-SC	Smagorinsky	Static Coarse	-	77,760

4.3 Computational Mesh, Initial Conditions, and Wall Treatment

The initial mesh created to simulate the THAI vessel in each case and used in all eight LES simulations consisted of 120 hexahedral blocks, containing 77,760 computational cells throughout the domain. This initial mesh was used directly in all static coarse mesh simulations. For the dynamic mesh simulations using the anisotropic AMR, two levels of mesh refinement were considered, which significantly increased the mesh resolution in the areas surrounding the flame front. A maximum of 4.98 million computational cells would be required to achieve the same level of mesh resolution if all grid blocks were refined isotropically and uniformly; however, in practice the mesh sizes for the dynamic AMR simulations did not exceed 900,000 cells, which corresponds to approximately 82% refinement efficiency.

The boundaries of the computational domain, representing the interior surfaces of the closed vessel, were taken to be isothermal no-slip boundaries. The no-slip boundary is modeled using an algebraic law-of-the-wall model [17]. For the isothermal condition, all walls were taken to have a constant temperature equal to that of the initial temperature of the reactant gases, and a thermal wall model [18] is used to better predict the heat flux through the walls. The unburnt gas mixture (c=0) and its temperature within the vessel corresponded to recorded values of the gas temperature and hydrogen and steam concentrations for the two THAI cases summarized in Table 1. The remaining component of the gas mixture within the vessel was assumed to be air as represented by a 21:79 oxygen-nitrogen mixture. The nominal value of the initial pressure was also made to match the recorded values for the experiment, with the gas pressure and density varying with height to recreate the gravity-induced gradients.

The initial mean velocity field were assumed to be zero everywhere within the vessel. Additionally, an initial turbulence field was applied for each LES case based on the work of Rogallo [19]. As per the recommendation of the ISP-49 report [1], the initial turbulence field for the simulations was generated such that u_{rms} is on the

order of 10^{-2} m/s. Figure 3 shows a cutaway of the initial computational mesh alongside a cross-sectional contour plot of the initial turbulent Mach number.

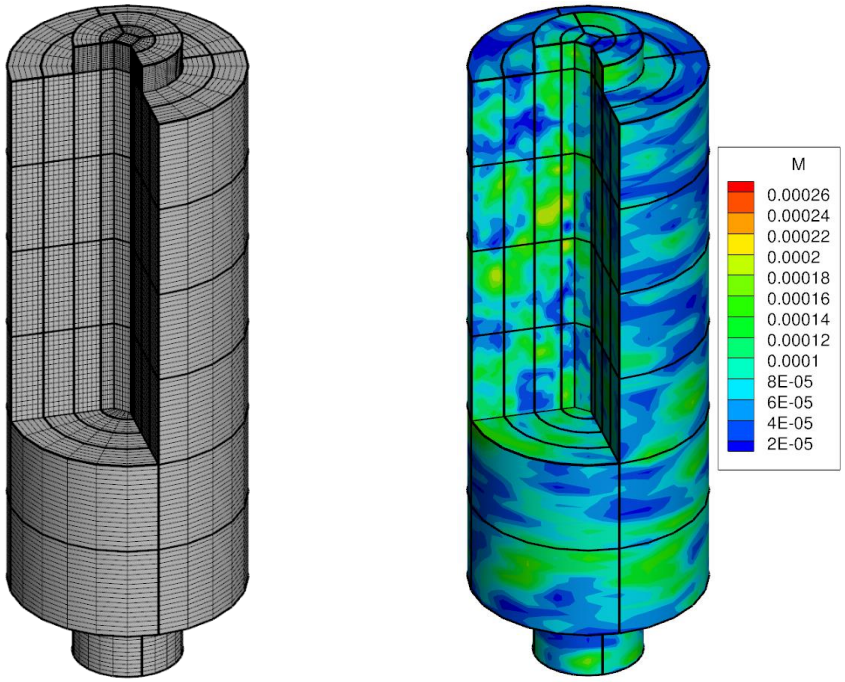

(a) (b)

Figure 3. a) Cutaway of initial mesh of the THAI vessel, and b) contour plot of the initial turbulence field Mach number on the same cutaway

4.4 Modelling of Ignition Process

The ignition process was simulated by using a forcing term to increase the value of the progress variable within a small volume within the lower cylinder of the vessel, centered on the vessel axis 50 cm above the base plate. The strength of the forcing term was taken to decay exponentially from the ignition point such that it approaches zero at a distance of 20 cm from the ignition point. The forcing term was also taken to decay gradually to zero within the first one second of simulated time.

5.0 LES RESULTS AND DISCUSSION

All LES simulations were performed using a homogeneous parallel cluster consisting of 1500 nodes where each node has 40 Intel 2.4 GHz CPU cores (for a total of 60,000 cores) and 202 GB of memory. The nodes are interconnected by a low-latency EDR Infiniband network. The static coarse mesh cases were performed using 120 cores of this cluster and the dynamic AMR mesh cases were performed using 600 cores. The solution state at 44 points in the vessel (corresponding to the "fast" thermocouples and one pressure sensor in the experimental case) was saved every 500 time steps, while the entire solution was saved every 250 ms of simulated time.

5.1 Flame Position and Propagation

The position of the flame was tracked along the THAI vessel's vertical axis as it propagated. In the experiments, the flame was considered to have "arrived" at a sensor when there was a sharp rise in temperature, distinguishing

from the gradual temperature rise due to global pressure increase; tracking the arrival of the flame was done in a similar fashion for the simulation cases considered. Figure 4 shows the flame progression of each of the THAI cases compared with the simulations.

Each case in Figure 4 is plotted according to simulated time, with t=0 s corresponding to the start of each simulation. However, since the experiments did not initiate the combustion precisely at the experimental t=0 s and the ignition model used in this work does not perfectly model the ignition process, the experimental data has thus been offset in time to account for the possible discrepancies in the ignition process and align the experimental data with the closest simulated data set to better compare the results. All times referred to in the following discussions correspond to this offset experimental time, which is referred to as the "adjusted" or "simulated" time.

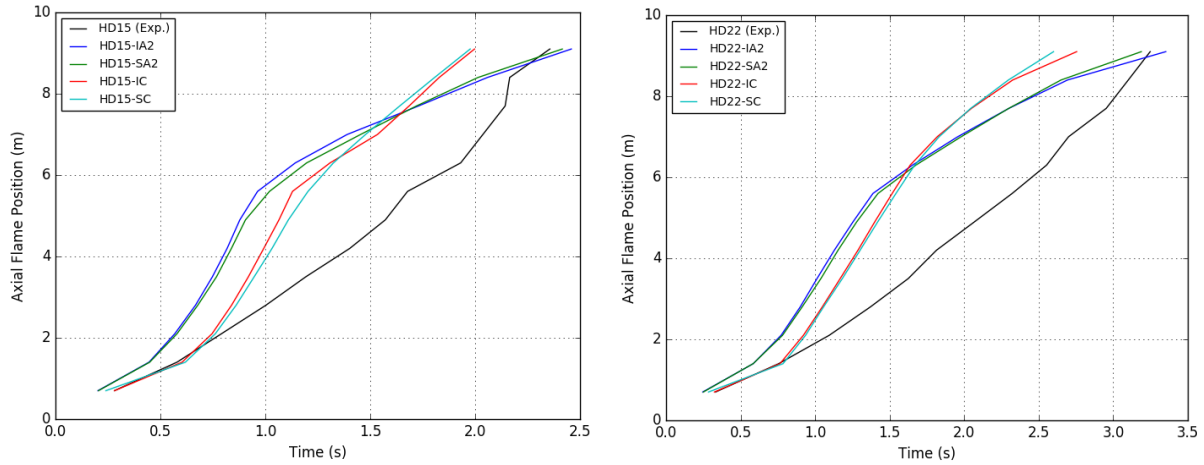

(a) (b)

Figure 4. Axial flame locations for each THAI experiment, with a) comparison of the HD15 cases and b) comparison of the HD22 cases.

In the HD15 simulation cases, all simulations predicted a higher flame speed beyond the 0.5-0.75 second mark than observed in the experiment. All simulations also showed a significant decrease in the axial flame velocity near the 1 second simulated time mark; this corresponds to the point where the mixture in the lower volumes of the vessel had completed burning such that effect of gas expansion on the flame propagation is reduced. Both AMR cases predicted a lower flame velocity than the static cases after the point of deceleration; the static cases tended to predict a flame speed similar to that seen in experiment, though the AMR cases better predicted the average flame speed. The Smagorinsky and ILSA models predicted broadly similar flame trends within the same AMR class, though the ILSA model tends to predict sharper variations in flame speed at the deceleration point.

The HD22 cases show similar trends to that of the HD15 cases: early over-acceleration of the flame accompanied by a deceleration mid-way through the deflagration. However, the static HD22 cases show much smoother transitions between the accelerating and decelerating regimes, whereas the AMR cases have a much sharper deceleration of the flame followed by a period of steady flame velocity. The AMR cases again show a better prediction of the average flame velocity over the whole deflagration, but in these cases the post-deceleration velocity more closely matches the experimental value. The HD22 cases showed significantly less differentiation between the ILSA and Smagorinsky cases than that seen in the HD15 cases.

In general, it would seem from the results for the HD15 and HD22 cases that the dynamic AMR LES results slightly overestimate the initial flame acceleration. This underestimation of the initial flame acceleration is likely

a result of the coarse mesh and its impact on the ignition model, as the coarse mesh prevents the ignition from being tightly focused on a very small region of space (as would be found using a spark igniter) and instead forcing the ignition to occur over a somewhat larger volume.

The HD22 experimental was selected as one of the blind-phase test cases considered in the ISP-49 report [1], allowing additional comparisons of the present simulation results to the previous CFD predictions of this blind study. The blind phase results were considered here as opposed to the open phase results, as the models used in this study were not modified or "tuned" to increase agreement with the experimental results, despite having *a priori* access to the THAI data. In general, the present LES results exhibit equivalent or better agreement with experiment than the previous simulation results of the ISP-49 study [1], although the current simulations tend to disagree with the measured data at the early stages of the deflagration beyond the 0.5-0.75 second mark.

5.2 Rate of Pressure Increase

In the THAI experiments, the pressure was measured by a sensor at a point next to the vessel wall at an elevation of 4.9 m [1]. Pressure values from the LES simulations were taken at the equivalent point within the computational domain; the simulated pressure histories are depicted in Figure 5 and compared to the corresponding measured values. The HD15 AMR and static mesh LES results predict a similar rate of pressure rise at the beginning stages of the experiment, although the static cases are delayed in time presumably due to the delayed ignition effect mentioned in the previous section. The static mesh cases show a consistent rate of pressure increase higher than that found in experiment, whereas the AMR cases show a distinct decrease in the rate of pressure increase at the 1 second mark, for reasons similar to that of the deceleration observed in the flame front at the same point, although the static cases do not show a corresponding feature. A similar decrease was found in experiment at a similar point. The predicted maximum pressure reached is very close to and just slightly higher than that found in experiment. The decrease in the pressure past the peak value, indicative of heat being lost to the walls, closely matches with the experiment. The differences between the ILSA and Smagorinsky cases do not produce a significant effect on the pressure history, with the Smagorinsky cases showing nominally higher rates of pressure increase such that the peak pressure is reached a fraction of a second earlier.

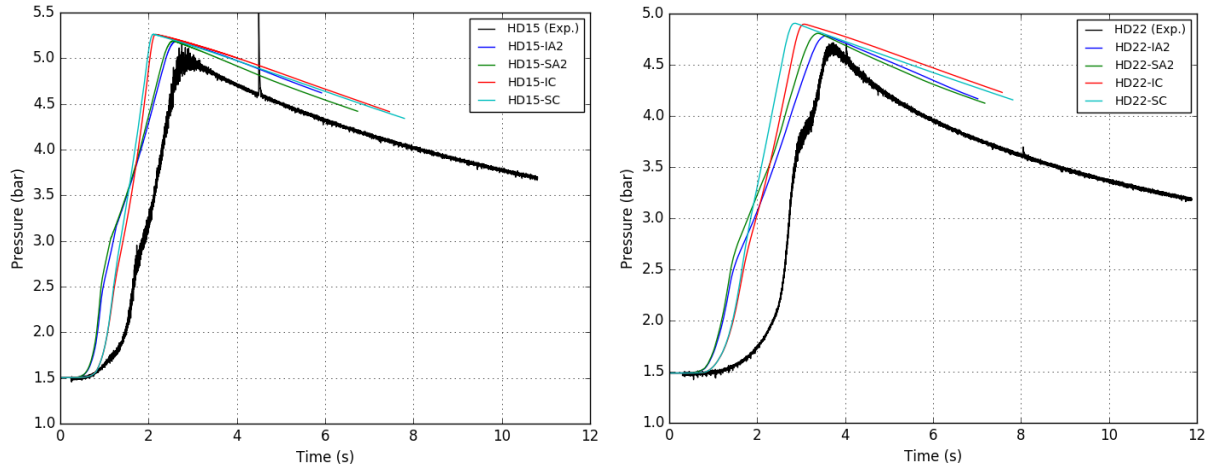

(a) (b)

Figure 5. Comparison of pressure predictions for each THAI experiment, with a) comparison of the HD15 cases and b) comparison of the HD22 cases.

The HD22 cases show similar trends to that of the HD15 cases in pressure history as well. Both AMR cases feature a reduction in the rate of pressure increase at approximately 1 second simulated time; however, in the experiment a similar trend is observed only later in the deflagration. The use of AMR improves the estimate of time and value of the peak pressure value, which is likely at least partially due to increased estimates of heat transfer at the wall. The differences between the Smagorinsky and ILSA models are larger than that seen in the HD15 case, though the differences remain minor.

As in the axial flame position results, the simulated deflagrations appear to be too strong in the early stages of the deflagration flame propagation while weakening in the later stages when compared with experimental results. This is shown by the early over-acceleration of the flame observed in the previous section and the earlier rise of pressure observed here. The rapid pressure rise and early over-acceleration of the flame might be the result of an over-estimation of the strength of the ignition process and the combustion process in the early stages of the deflagration. This is supported by considering the comparison of the experimental and simulated temperatures observed along the vessel axis, as seen in Figure 6. The experimental results show gradual increases in temperature and lower peak temperature values, whereas the simulation results show rapid increases in temperature and higher peak temperatures, which could result from a lack of a radiative heat transfer model or insufficient mixing when compared to experiment. This would increase the buoyant force on the burned region to increase the early velocity of the flame, among other effects. Alternatively, this could be the result of instrumentation, though the extent to which the response times of the thermocouples used may have influenced the data is unclear.

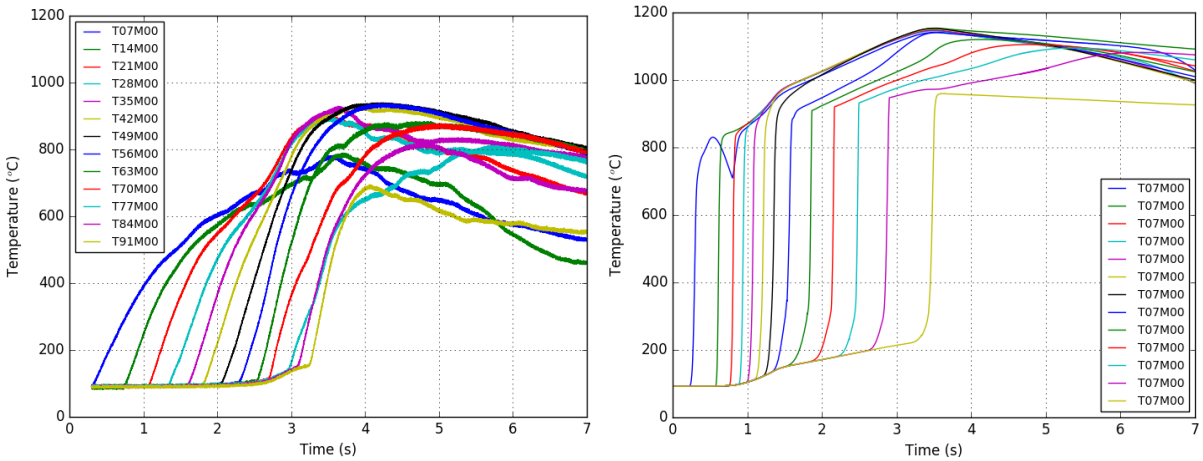

Figure 6. Comparison of axial temperatures recorded for the HD22 case, with a) experimental values and b) the HD22-IA simulated values. Each plotted line corresponds to a thermocouple at a height denoted by the first two numbers in the sensor name in decimetres. For instance, T35M00 is located 3.5 meters above the vessel floor.

The weakening of the deflagration toward the late stages of the simulation might arise from the lack of large-scale flame wrinkling observed in the simulations. This is likely due to the limitations of the BVM model and the fact that the flame front is artificially thickened on the coarse mesh, as shown in Figure 7, producing a smaller overall volume of burned products and therefore, resulting in lower pressures despite similar flame front locations. As also shown in Figure 7, the use of AMR reduces the flame thickness and enables higher levels of flame curvature, but has not produced wrinkling at the flame front. Higher levels of AMR may allow the flame to grow thin enough to wrinkle more substantially and develop finer-scale features. If a substantially wrinkled flame is developed early in the simulation it may also enhance the transfer of heat to the walls and reduce the strength of the deflagration in the early stages of the simulation.

In general, the LES predictions of the present study were again similar to those of the previous blind-study summarized in the ISP-49 report [1]. In particular, the predictions for the rates of pressure rise obtained in the present HD22 simulations exceed many of the predictions given in the ISP-49 report and when considering the agreement with experimental data as discussed above, it is felt that the present LES results show a marked improvement over the results given in the ISP-49 report [1].

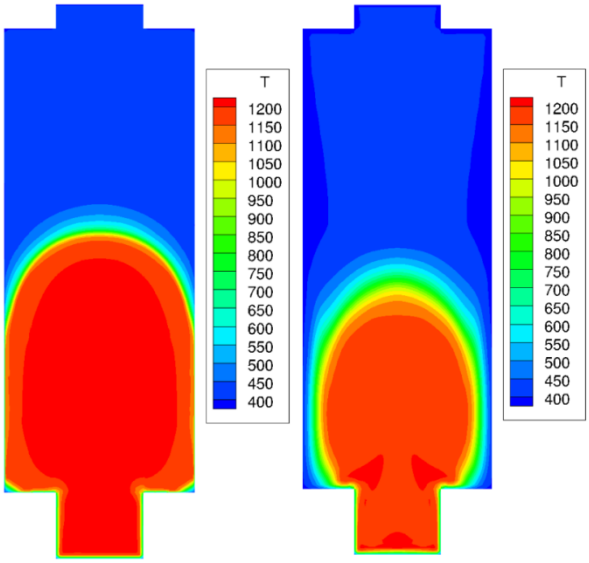

(a) (b)

Figure 7. Comparison of a) HD22-IA and b) HD22-IC at 1.5 seconds simulated time.

6.0 CONCLUSIONS AND FUTURE RESEARCH

A novel block-based anisotropic AMR method has been applied in conjunction with a recently proposed mesh-independent ILSA SFS model for preforming LES of turbulent premixed hydrogen flames in closed vessels. LES results were obtained and compared to available data for several well-known THAI experiments. In particular, the predicted vertical flame height and vessel pressure histories were compared with experiment. In general, reasonable agreement with experiment was observed for the predictions of the pressure increase and, as would be expected, use of AMR generally improved the agreement between simulation and experiment and introduced behaviour in the pressure histories observed in experiment and not in the static cases. The LES results tended to predict similar rates of pressure increase while providing reasonable estimates of the peak pressure and pressure decrease past the peak. While the performances of the ILSA and Smagorinsky models were comparable, it is felt that the ILSA model provided a more consistent behavior for the various meshes considered herein. Further study of the potential of the proposed LES approach for hydrogen deflagration prediction in closed vessels will continue in future research by considering a wider range of the THAI experiments.

7.0 ACKNOWLEDGEMENT

The authors gratefully acknowledges the joint financial support of the hosting country (Germany) and the participating countries for the OECD/NEA sponsored THAI project and support from Canadian Nuclear Laboratories, under the auspices of the New Technology Initiatives Fund. Computational resources for performing all of the calculations reported herein were provided by the SciNet High Performance Computing Consortium at the University of Toronto and Compute/Calcul Canada through funding from the Canada Foundation for Innovation and the Province of Ontario, Canada.

8.0 REFERENCES

[1] "ISP-49 on Hydrogen Combustion," Nuclear Energy Agency, JT03314550, 2012.

[2] M. J. Williamschen and C. P. T. Groth, "Parallel Anisotropic Block-Based Adaptive Mesh Refinement Algorithm For Three-Dimsensional Flows," AIAA Paper 2013-2442, June 2013.

[3] L. Freret and C. P. T. Groth, "Anisotropic Non-Uniform Block-Based Adaptive Mesh Refinement Algorithm for Three-Dimensional Inviscid and Viscous Flows," AIAA Paper 2015-2613, June 2015.

[4] S. B. Pope, "Ten Questions Concerning the Large-Eddy Simulation of Turbulent Flows," *New Journal of Physics,* vol. 6, 2004.

[5] L. Freret, L. Ivan, H. De Sterck and C. Groth, "A High-Order Finite-Volume Method with Anisotropic AMR for Ideal MHD Flows," AIAA Paper 2017-0845, January, 2017.

[6] L. Freret, C. P. T. Groth, T. B. Nguyen and H. De Sterck, "High-Order Finite-Volume Scheme with Anisotropic Adaptive Mesh Refinement: Efficient Inexact Newton Method for Steady Three-Dimensional Flows," AIAA Paper 2017-3297, June 2017.

[7] L. Freret, L. Ivan, H. De Sterck and C. P. T. Groth, "High-Order Finite-Volume Method with Block-Based AMR for Magnetohydrodynamics Flows," *Journal of Scientific Computing,* pp. doi.org/10.1007/s10915-018-0844-1, 2018.

[8] U. Piomelli, A. Rouhi and B. J. Geurts, "A Dynamic Subfiltre-Scale Stress Model for Large Eddy Simulation," *Physical Review Fluids,* vol. 766, 2016.

[9] J. Smagorinski, "General Circulation Experiments with te Primitive Equations. I: The Basic Experiment," *Monthly Weather Review,* vol. 91, no. 3, pp. 99-165, 1963.

[10] F. E. Hernandez-Perez, F. T. C. Yue, C. P. T. Groth and O. L. Gulder, "LES of a Laboratory-Scale Turbulent Premixed Bunsen Flame Using FSD, PCM-FPI and Thickened Flame Models," *Proceedings of the Combustion Institute,* vol. 33, pp. 1365-1371, 2011.

[11] F. E. Hernandez-Perez, C. P. T. Groth and O. L. Gulder, "Large-Eddy Simulation of Lean Hydrogen-Methane Turbulent Premixed Flames in the Methane-Dominated Regime," *International Journal of Hydrogen Energy,* vol. 39, pp. 7147-7157, 2014.

[12] N. Shahbazian, M. M. Salehi, C. P. T. Groth and O. L. B. W. K. Gulder, "Performance of Conditional Source-Term Estimation Model for LES of Turbulent Premixed Flames in Thin Reaction Zones Regime," *Proceedings of the Combustion Institute,* vol. 35, pp. 1367-1375, 2015.

[13] V. Molkov and M. Bragin, "Hydrogen-Air Deflagrations: Vent Sizing Correlation for Low-Strength Equipment and Buildings," *International Journal of Hydrogen Energy,* vol. 40, no. 2, 2015.

[14] "CANTERA Release 1.8," California Institute of Technology, 2009. [Online]. Available: http://code.google.com/p/cantera.

[15] V. A. Alekseev, M. Christensen and A. A. Konnov, "The effect of temperature on the adiabatic burning velocities of diluted hydrogen flames: A kinetic study using an updated mechanism," *Combustion and Flame,* vol. 162, 2015.

[16] P. L. Roe, "Approximate Riemann Solvers, Parameter Vectors and Difference Schemes," *Journal of Computational Physics,* vol. 43, pp. 357-372, 1981.

[17] "Wall Stress Models," University of Maryland, [Online]. Available: http://wmles.umd.edu/wall-stress-models/. [Accessed November 2018].

[18] C. Angelberger, T. Poinsot and B. Delhay, "Improving near-wall combustion and wall heat transfer in SI engine computations," *SAE Technical Paper 972881,* 1997.

[19] R. S. Rogallo, "Numerical Experiments in Homogeneous Turbulence," NASA, NASA-TM-81315, 1981.